Quasielastic neutron scattering probing H⁻ dynamics in the H⁻ conductors LaH₃₋₂ₓOₓ

Hiromu Tamatsukuri [1,*] Keiga Fukui,[2] Soshi Iimura,[3,4,5] Takashi Honda,[6,7] Tomofumi Tada,[3,8] Youichi Murakami,[3,6]
Jun-ichi Yamaura [3] Yoshio Kuramoto,[6] Hajime Sagayama,[6,7] Takeshi Yamada [9] Masato Matsuura,[9] Kaoru Shibata [1,†]
Maiko Kofu,[1] Yukinobu Kawakita,[1] Kazutaka Ikeda,[6,7] Toshiya Otomo,[6,7] and Hideo Hosono[3,5]

¹*Materials and Life Science Division, J-PARC Center, Japan Atomic Energy Agency, Tokai, Ibaraki 319-1195, Japan*
²*Graduate Faculty of Interdisciplinary Research, University of Yamanashi, 4-3-11 Takeda, Kofu 400-8511, Japan*
³*Materials Research Center for Element Strategy, Tokyo Institute of Technology, Yokohama, Kanagawa 226-8503, Japan*
⁴*PRESTO, Japan Science and Technology Agency, Kawaguchi, Saitama 332-0012, Japan*
⁵*National Institute for Materials Science (NIMS), Tsukuba, Ibaraki 305-0047, Japan*
⁶*Institute of Materials Structure Science, High Energy Accelerator Research Organization (KEK), Tsukuba 305-0801, Japan*
⁷*Department of Materials Structure Science, The graduate University for Advanced Studies, Tsukuba 305-0801, Japan*
⁸*Kyushu University Platform of Inter/Transdisciplinary Energy Research, Kyushu University, Fukuoka 819-0395, Japan*
⁹*Neutron Science and Technology Center, Comprehensive Research Organization for Science and Society (CROSS),
Tokai, Ibaraki 319-1106, Japan*

Using an incoherent quasielastic neutron scattering (QENS) technique, we investigate H⁻ dynamics in a series of oxyhydrides LaH₃₋₂ₓOₓ that exhibit characteristic high H⁻ conductivity. In the end member LaH₃ ($x = 0$), two kinds of H⁻ dynamics are identified: the jump diffusion and the localized motion. The jump length in the jump diffusion mode increases with increasing T. The localized motion is identified as a jump between the two inequivalent sites. These dynamics are corroborated by our molecular dynamical simulations. Our QENS data suggest that similar H⁻ dynamics occurs also in oxyhydrides LaH₃₋₂ₓOₓ ($x \neq 0$), whose H⁻ concentration dependence is consistent with the previous measurement of ionic conductivity. We also discuss the possibility that LaH₃₋₂ₓOₓ is an example of H⁻ ion conductors governed by the concerted migration mechanism. The identified H⁻ dynamics is key to understanding the anomalous hydrogen concentration dependence of the diffusion coefficient in lanthanum hydrides, which has been a longstanding mystery in this compound.

I. INTRODUCTION

Hydrogen is widely known to exhibit very large diffusion coefficients in metals. For example, the diffusion coefficient of hydrogen in a body-centered cubic Fe metal reaches $10^{-9} \sim 10^{-8}$ m²/s around 300 K, which is comparable with atomic diffusion in liquids at room temperature [1]. Understanding the large hydrogen diffusion coefficients in metals is not only essential for industrial use of materials, as exemplified by hydrogen embrittlement (hydrogen-induced cracking) and hydrogen storage, etc., but also has attracted fundamental interest in anomalous hydrogen diffusion, which is partly due to the strong quantum properties of hydrogen.

In metals with low solid solubility of hydrogen, such as Cu, Ni, and Fe, hydrogen migrates through interstitial spaces, specifically, a tetrahedral site or an octahedral site composed of the metal frameworks [1]. In the case of metals with high hydrogen solubility, hydrogen gradually fills the interstitial spaces with increasing concentration of hydrogen and then, forms stoichiometric hydrides, e.g., TiH₂ and ZrH₂. As a result, the hydrogen diffusion coefficient at a given tem-

perature goes to zero when the interstitial spaces are fully occupied [2,3]. Strangely, in contrast, a diffusion coefficient of hydrogen in LaHₓ′ ($2 \leqslant x' \leqslant 3$) continues to increase with increasing x' [4]. Similar tendency is also observed in YHₓ′ ($1.8 \leqslant x' \leqslant 2.1$) [3]. Although a collective motion of hydrogens is suggested for the origin of these anomalous diffusions, much remains unclear about microscopic hydrogen dynamics in LaHₓ′.

Recently, Fukui *et al.* reported high conductivities of hydrogen ions in a series of oxyhydrides LaH₃₋₂ₓOₓ ($x \neq 0$), which are derivative materials of LaH₃ by a partial substitution of O²⁻ ions for hydrogen ions [5,6]. They have also established that a conductive hydrogen in these materials is not a proton H⁺, but a hydride ion H⁻ [5,6]. Because the diffusion coefficients of H⁻ in these materials, especially with $x < 0.25$, are comparable to those in LaHₓ′ [4,6], a similar H⁻ conduction mechanism is expected. Elucidation of unique H⁻ dynamics in LaHₓ′ and LaH₃₋₂ₓOₓ will provide useful guidelines for designing other H⁻ conductive materials, which have growing interest for their potential to realize novel energy storage and conversion devices with high energy densities [7–14].

An incoherent quasielastic neutron scattering (QENS) technique is a powerful method to investigate microscopic ion dynamics [15,16]. Because the incoherent scattering function is derived from the self-correlation function, the incoherent QENS can directly measure dynamics of 'each' mobile ion,

---

*hiromu.tamatsukuri@j-parc.jp
†Present address: Division of Neutron Application Technology, Radiation Application Development Association, Tokai, Ibaraki 319-1106, Japan.

184114-1

such as self-diffusion and atomic localized motion [15,16]. In this paper, we apply the incoherent QENS technique to investigation of H^- dynamics in a lanthanum hydride $LaH_{3-\delta}$ with $\delta < 0.09$ and oxyhydrides $LaH_{3-2x}O_x$. We identify two kinds of microscopic H^- dynamics in the end member $LaH_{3-\delta}$; a jump diffusion with increase of diffusion length on increasing T, and a back-and-forth jump between neighboring tetrahedral and octahedral sites, which would be key dynamics to the anomalous x' dependence of the diffusion coefficient in $LaH_{x'}$. These dynamics are corroborated by our molecular dynamical (MD) simulations. Although the QENS intensities are smaller, the H^- dynamics in oxyhydrides $LaH_{3-2x}O_x$ ($x \neq 0$) looks similar to that in $LaH_{3-\delta}$. We also discuss that the origin of the high H^- conductivity in this system is explained by a so-called caterpillar model or a concerted migration model.

II. EXPERIMENTS AND ANALYSES

All of the samples used in this study are polycrystalline powder form. The details of the synthesis are described in Ref. [5]. For the QENS measurements, the powder samples were wrapped in Al foils under the He atmosphere, and then the Al foils in the form of the cylindrical shape were inserted and sealed in an Al sample cell with He gas. To reduce the neutron transmittance to 90%, we use $La_4H_4O_4$, $La_4H_6O_3$, $La_4H_8O_2$, and $LaH_{3-\delta}$, with the weights of 5.11, 3.68, 2.68, and 1.69 g, respectively (see below about notation of these chemical formula). The corresponding thicknesses of the samples after wrapping the Al foils are roughly 0.55, 0.4, 0.3, and 0.2 mm, respectively. The proportions of the incoherent scattering cross section of H to the total cross section of $La_4H_4O_4$, $La_4H_6O_3$, $La_4H_8O_2$, and $LaH_{3-\delta}$ are 63.4%, 72%, 77.3%, and 83.4%, respectively, while those of the coherent one are 1.4%, 1.6%, 1.7%, and 1.8%. Therefore, almost all QENS signals from H originate from the incoherent scatterings. The QENS measurements with the time-of-flight method were performed using the near-backscattering spectrometer with high energy resolution, DNA, installed at BL02 [17], and the cold-neutron disk chopper spectrometer, AMATERAS, installed at BL14 [18], in the Materials and Life Science Experimental Facility (MLF) of the Japan Proton Accelerator Research Complex (J-PARC). In the experiments at DNA, the final neutron energy of 2.08 meV was selected using Si (111) analyzers. A frequency of the pulse-shaping choppers and their slit sizes were set to 225 Hz and 3 cm × 3 cm, respectively, which leads to the energy resolution of 3.6 μeV at $E = 0$ eV (full width at half maximum) and the observable energy range of -40 μeV $\leqslant E \leqslant 100$ μeV. These conditions enable us to investigate the migration dynamics in a time range about between 40 ps and 1.15 ns. The chopper setting employed in the experiments at AMATERAS enabled us to simultaneously obtain the data for the incident energies E_i's of 7.7, 3.1, and 1.7 meV (the multi-E_i mode [18]) with the energy resolutions of 0.21, 0.055, and 0.023 meV at $E = 0$ eV (full width at half maximum), respectively. The resolution functions of each sample were measured below 10 K in both experiments. Note that the highest temperatures in each sample are below the hydrogen desorption temperatures [5].

The time-of-flight data were converted to a neutron scattering function $S(Q, E)$ map and analyzed using the UTSUSEMI software [19].

The measured $S(Q, E)$ was fitted to the following function:

$$S(Q, E) = A_0(Q)\delta(E) + A_1(Q)L_1(Q, E)$$
$$+ A_2(Q)L_2(Q, E) + C_{B.G.}, \quad (1)$$

convoluted with the resolution function $R(Q, E)$. The delta function $\delta(E)$ describes the elastic component, which includes the contribution from the sample cell and the instruments, and $C_{B.G.}$ is the constant background. In our data, QENS components are described by the Lorentz function $L_i(Q, E)$ ($i = 1, 2$),

$$L_i(Q, E) = \frac{1}{\pi} \cdot \frac{\Gamma_i(Q)/2}{E^2 + [\Gamma_i(Q)/2]^2}, \quad (2)$$

where Γ_i is the full width at half maximum (FWHM) of the Lorentzian. A_j's ($j = 0, 1,$ and 2) measure the strength of each component. The fitting procedures were performed using the PAN program in the DAVE software package [20].

Neutron diffraction measurement for the deuterated LaD_3 was carried out using the high-intensity total diffractometer (NOVA) installed at BL21 in MLF, J-PARC. The sample with the weight of 1.32 g was sealed into a sample cell composed of V 96.4%-Ni 3.6% (with an outer (inner) diameter 6 (5.8) mm) under the Ar atmosphere. The FULLPROF software was used for the Rietveld analysis [21]. The image of the crystal structure in Supplemental Material (SM) [22] Sec. A was generated using the VESTA software developed by Momma and Izumi [23].

III. RESULTS AND DISCUSSION

A. Crystal structures and typical neutron scattering results of $LaH_{3-2x}O_x$

First, we describe the crystal structures of the target compounds, $LaH_{3-2x}O_x$, and introduce another notation of their chemical formulas. As shown in Fig. 1(a), LaH_3 crystallizes in an α-BiF_3 type structure with space group $Fm\bar{3}m$, in which La^{3+} ions form a face-centered-cubic (f.c.c.) lattice. There are two kinds of anion sites, the tetrahedral (Tet) and the octahedral (Oct) sites, center of the La_4 tetrahedron and La_6 octahedron, respectively [4,24,25]. Note that LaH_3 tends to have a small number of H^- defects [4,24]. Indeed, our sample used in this article is determined as $LaH_{3-\delta}$ with $\delta < 0.09$. As long as $\delta \neq 0$, our conclusions do not depend on the precise value of δ. As revealed by the previous study [5], a partial substitution of O^{2-} for H^- introduces a vacant site to preserve charge neutrality and leads to slight distortion from the La f.c.c. lattice to a tetragonal lattice ($P4/nmm$). However, the tetragonality is quite small [5]. Thus, we employ the pseudo-f.c.c. unit cell in this article to make a comparison easier. Accordingly, notation of chemical formulas of the oxyhydrides are replaced with $La_4H_yO_{(12-y)/2}$ ($4 \leqslant y \leqslant 12$) to explicitly show the number of H^- in the pseudo-f.c.c. unit cell. In short, $LaH_2O_{0.5}$ ($x = 0.5$) and $LaHO$ ($x = 1$) in the literature [5] correspond to $La_4H_8O_2$ and $La_4H_4O_4$ in this paper, respectively. As determined by the previous study [5], O^{2-} and H^- preferentially occupy the Tet sites, and remaining
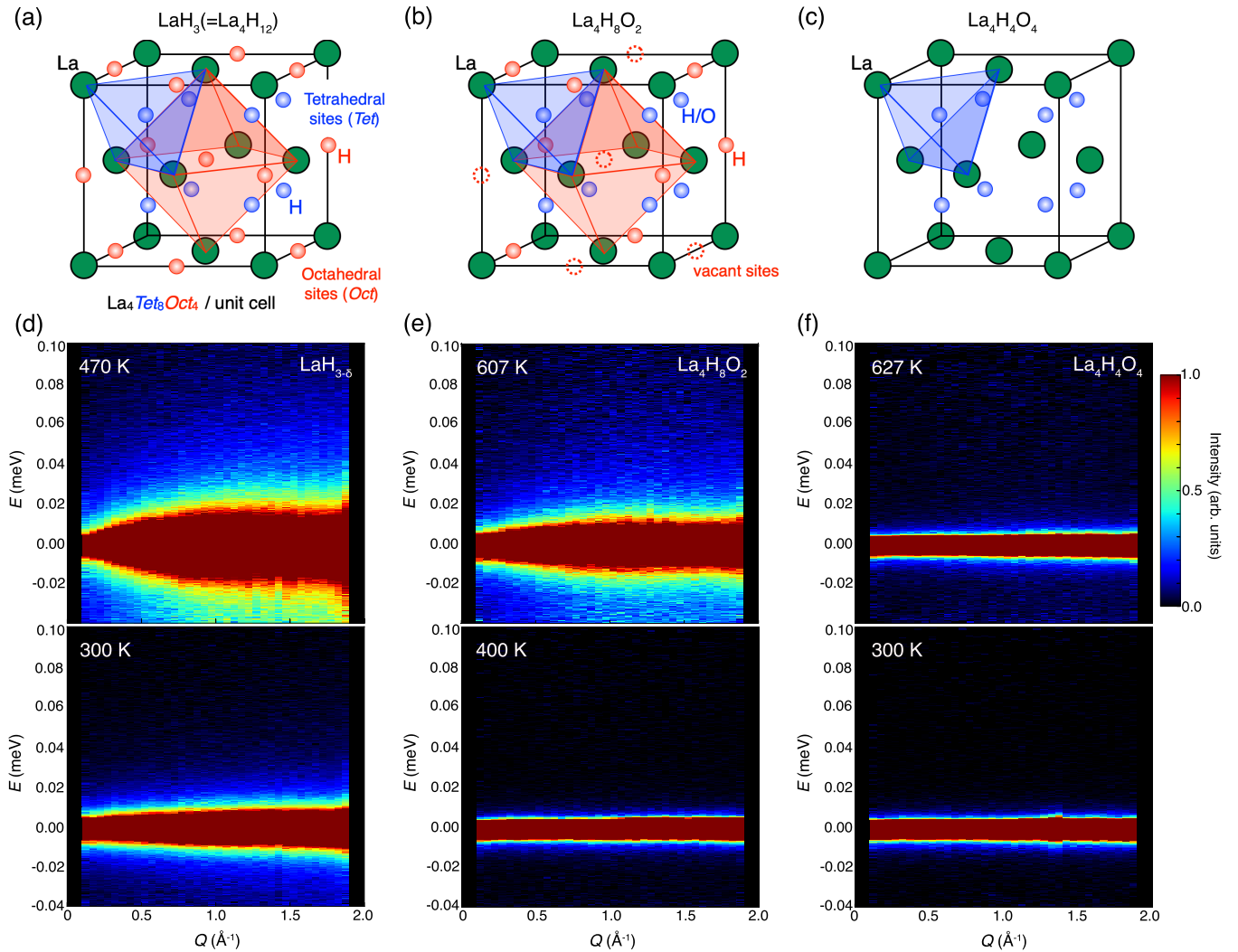
FIG. 1. (a)–(c) Crystal structures of (a) LaH_3, (b) $La_4H_8O_2$, and (c) $La_4H_4O_4$, with a convenient unit cell that we use in this article. Although an original lattice system of $La_4H_8O_2$ and $La_4H_4O_4$ is tetragonal ($P4/nmm$), La ions approximately form the f.c.c. unit cell. (d)–(f) Typical $S(Q, E)$ maps of (d) $LaH_{3-\delta}$, (e) $La_4H_8O_2$, and (f) $La_4H_4O_4$. The data shown in upper panels are results at each of the highest temperatures in the experiments. For visibility, intensities of the data for $LaH_{3-\delta}$ are multiplied by 0.5. Note that rather large seeps of intensities around $Q = 2.0$ Å^{-1} in $LaH_{3-\delta}$ are due to the Bragg reflection.

H^- occupy the Oct sites in these compounds, namely, in $La_4H_4O_4$, $4O^{2-}$ and $4H^-$ occupy the Tet sites and the Oct sites are vacant [Fig. 1(c)], while in $La_4H_8O_2$, $2O^{2-}$ and $6H^-$ occupy the Tet sites and the remaining $2H^-$ occupy the Oct sites [Fig. 1(b)].

Figures 1(d)–1(f) show the typical neutron scattering function, $S(Q, E)$, of these compounds as a function of momentum (Q) and energy (E) transfers. The data of $La_4H_8O_2$ [Fig. 1(e)] are representative of QENS data; at 400 K, only incoherent elastic scattering is observed (no Bragg peak in this Q range), whereas at 607 K, a broad symmetric incoherent quasielastic scattering due to a H^- migration appears (the incoherent scattering cross section of oxygen is 0). With smaller intensities, similar feature can be seen in $La_4H_4O_4$ [Fig. 1(f)]. In the end member $LaH_{3-\delta}$ [Fig. 1(d)], more conspicuous QENS spectra are observed and, moreover, the H^- migration occurs even at 300 K, although there are only a small number of vacant Oct sites to hop over in this compound. As shown in SM Sec. D [22], the H^- migration

in $LaH_{3-\delta}$ starts at such low temperature as 175 K. These results indicate that the key factor in the high mobility of H^- in $La_4H_yO_{(12-y)/2}$ is a concentration of H^-. On the other hand, our MD simulation shows that the H^- migration does not occur in LaH_3 ($\delta = 0$) even at 473 K, whereas the slight H^- defects with $\delta = 0.02$, 0.01, and 0.002 cause the H^- migration (see SM Sec. F [22]). Therefore, the small number of the vacant Oct sites is also essential for H^- migrations.

B. Fitting results of the $S(Q, E)$ spectra for $LaH_{3-\delta}$

First, we focus on the H^- dynamics in $LaH_{3-\delta}$. As shown in Fig. 2, the $S(Q, E)$ spectra of $LaH_{3-\delta}$ above 300 K are well fitted by introducing the two kinds of Lorentzian components, $L_{1(2)}$. The FWHM of L_1 shows characteristic Q dependence as will be shown later, while that of L_2 are almost independent of Q as shown in the inset of Fig. 2. These features corroborate a jump diffusion mode (L_1) and a localized mode (L_2), respectively [15,16].
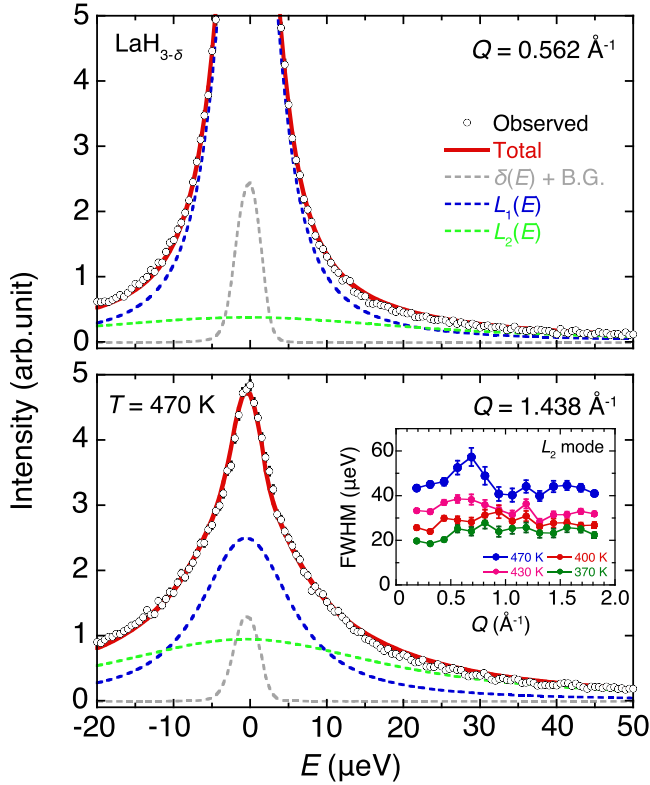
FIG. 2. Typical fitting results of the $S(Q, E)$ spectra for LaH$_{3-\delta}$ at 470 K. An inset shows Q dependence of a full width at half maximum (FWHM) of L_2 at several temperatures.

Figure 3(a) shows the Q dependence of the FWHM $\Gamma(Q)$ of L_1. To parametrize this diffusion process, we use the Chudley-Elliott model as a fitting function, which is the simplest one to describe the jump diffusion [15,16,26],

$$\Gamma(Q) = \frac{2\hbar}{\tau}\left(1 - \frac{\sin Ql}{Ql}\right), \qquad (3)$$

where τ and l are a residence time and a jump length, respectively. The fitting is in excellent agreement, provided that the fitting parameter l gradually increases with increasing temperature, as shown in Fig. 3(b). It should be noted that this result does not straightforwardly correspond to a jump length of the H$^-$ diffusion in LaH$_{3-\delta}$ because the Chudley-Elliott model only describes a jump diffusion between equivalent sites. Because the length between the Tet and (adjacent) Oct sites is the shortest in LaH$_{3-\delta}$, we can assume that H$^-$ ions always migrate through this path as an elementary jump process, which is consistent with our MD simulation. This migration path is often assumed in discussing anion dynamics in several compounds in which host metals form an f.c.c. lattice, such as PdH$_x$ [27–30] and fluorite-type compounds [13,31]. A possible interpretation of the increase of l is as follows: At lower T, the H$^-$ migration that looks like the jump between the Tet sites is dominant in the timescale of our measurement, although the elementary jump process is the jump between the Tet and (adjacent) Oct sites; with increasing T, the proportion of the H$^-$ migration that looks like the jump between the Oct sites increases owing to the growing thermal fluctuation. Note that the crystal structure of LaH$_{3-\delta}$ does not change with

increasing T (see SM Sec. A [22]). Such an increase of l in the diffusion mode is also observed in several hydrides [32,33].

The diffusion constant, D, is related to τ and l as $D = l^2/(6\tau)$. The obtained value of D at 470 K is 3.5 $\times\ 10^{-10}$ m^2/s, which is consistent with the previous nuclear magnetic resonance results for LaH$_{2.92}$ (2.5 $\times\ 10^{-10}$ m^2/s at 500 K) [4]. The T dependence of D follows the Arrhenius law [$D = D_0\exp(-E_a/k_BT)$] and the activation energy E_a^{diff} of this H$^-$ diffusion process is deduced as 159(18) meV [Fig. 3(c)]. This value also agrees well with the reported activation energy (enthalpy) of LaH$_{2.92}$ (170 meV) [4].

The localized motion can be analyzed and described by the Q dependence of the elastic incoherent structure factor, EISF(Q), which is originally defined as $A_0/(A_0 + A_2)$ [15,16]. However, the diffusion component A_1 with a tiny width also exists and A_0 is difficult to extract from our QENS data for several temperatures. Therefore, following Ref. [34], we modify the definition of EISF(Q) to account for the resolution-limited diffusion mode. This definition is based on the condition that only A_2 contributes to $1 - \mathrm{EISF}(Q)$, and thus EISF(Q) is given by $(A_0 + A_1)/(A_0 + A_1 + A_2)$ [34].

The EISF(Q) deduced is shown in Fig. 3(d). The best fit to EISF(Q) is accomplished by a model with the jump between Tet and Oct sites:

$$\mathrm{EISF}(Q) = \frac{1}{(1+\rho)^2}(1 + \rho^2 + 2\rho\, j_0(Qd)), \qquad (4)$$

where $j_0(x) = \sin x/x$ is the spherical Bessel function of the zeroth order and $d = 2.43$ Å (fixed) is the jump length between the Tet and Oct sites. ρ is a ratio of mean residence times. The reciprocal of the residence time in each site corresponds to a jumping rate. Since the residence time at the Tet sites is longer than that at the Oct sites, ρ is defined as $\tau_{\mathrm{Oct}}/\tau_{\mathrm{Tet}}$. As shown in Fig. 3(e), ρ increases with increasing T. This indicates that at lower T, τ_{Tet} is much longer than τ_{Oct}, while with increasing T, they become similar to each other due to the growing thermal fluctuation. We find that the Q averaged FWHM of L_2 also follows the Arrhenius law [Fig. 3(f)], which gives the activation energy $E_a^{\mathrm{loc}} = 101(9)$ meV of this localized mode.

C. Discussion of H$^-$ dynamics in LaH$_{3-\delta}$

The Lorentzian width Γ_2 of the L_2 mode is characterized by the two main features: (i) Γ_2 depends little on Q (Fig. 2, inset) and (ii) Γ_2 obeys the Arrhenius law with the activation energy $E_a^{\mathrm{loc}} \sim 100$ meV [Fig. 3(f)]. Feature (i) suggests an essentially localized character of the relaxation while (ii) necessitates a potential barrier in the relaxation process. If the barrier is along the hopping path of H$^-$ from a Tet site to one of neighboring Oct sites, the local relaxation means that the relevant H$^-$ must come back to the original Tet site. Otherwise, the jumping motion contradicts feature (i) and such motion is in fact described by the jump-diffusion process in the Chudley-Elliott model.

Since H$^-$ ions have large electronic polarizability [5,6], a move of H$^-$ would cause a deformation of the La framework. The timescale of the fluctuations (vibrations) of La^{3+} ions should be longer than those of H$^-$ ions because of the much larger mass. Thus, this deformation of the La framework would break the translational symmetry in the timescale of
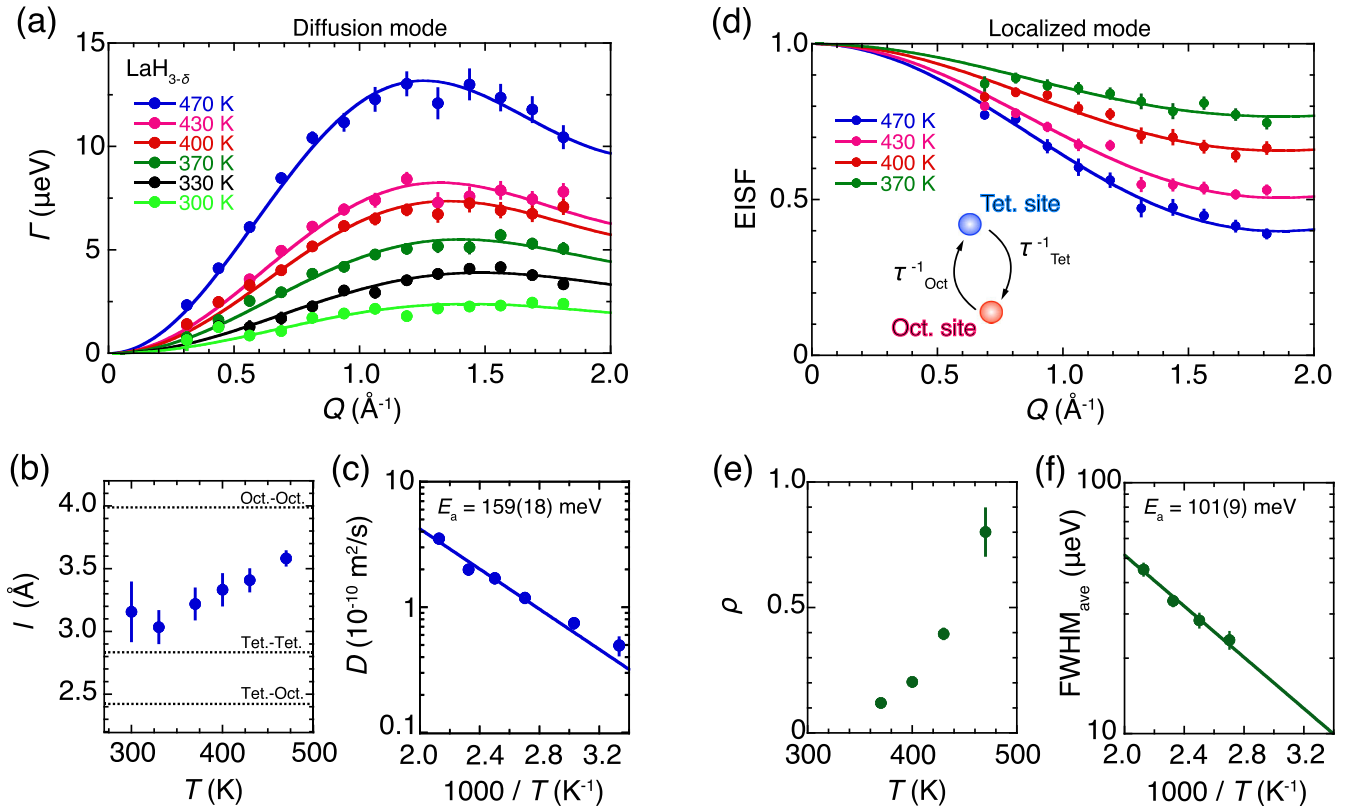
FIG. 3. (a) Q dependence of the FWHM of L_1 above 300 K. The solid curves are the fitting results of the Chudley-Elliott (C.-E.) model. (b) T dependence of the jump length l determined by the C.-E. model fitting. (c) Arrhenius plot of the diffusion coefficient D. Note that the residence time τ itself follows the Arrhenius law. However, because l also changes with changing T, the activation energy is derived from the T^{-1} dependence of D. (d) Q dependence of the elastic incoherent structure factor, EISF. The solid curves are the fitting results of the jump model between two inequivalent sites. The data of 300 and 330 K are omitted since they are rather scattered due to the small intensities. Inset shows the reciprocal of the residence time corresponding to the jumping rate. (e) T dependence of a ratio, $\rho \equiv \tau_{Oct}/\tau_{Tet}$ of the residence times τ_{Oct} and τ_{Tet} in the localized mode. (f) T^{-1} dependence of FWHM of L_2, which are averaged over Q measured. Error bars are estimated from the standard deviations in fitting.

the H^- migration. To investigate the dynamics of La^{3+} and H^- ions and local events in the atomistic point of view, we constructed DFT-based neural network potential (NNP) [35,36] for $LaH_{3-\delta}$, and analyzed the H^- migration barriers using the climbing image nudged elastic band method (CI-NEB) [37] with the DFT-NNP. The details of the computational conditions are shown in SM Sec. E [22]. First, we calculated the migration barrier for a single H^- jump from a Tet site to the nearest Oct site, and obtained the migration barrier for the single jump as 0.11 eV (see Fig. S7(c) in the SM [22]), whose value agrees well with $E_a^{loc} = 101(9)$ meV. According to the CI-NEB calculation, the H^- at the Tet site jumps into an off-center position of the neighboring vacant Oct site, which is unexpectedly closer to the Tet center. As a result, the emptied Tet site can be filled again more likely by the returning H^- rather than by another H^- at near Oct sites. The ensuing two-site processes will be the origin of the localized mode. On the other hand, we also obtained another event in which the vacant Tet site is promptly occupied by an H^- from another Oct site. The event is composed of two steps: (i) the first H^- jump (Tet to an off-center Oct) and (ii) the second H^- jump (Oct to the vacant Tet site), which show the barriers of 0.11 and 0.04 eV, respectively (Figs. S7(a) and S7(b) in the SM [22]). For the timescale of our QENS

measurement, a series of this process would be observed as the diffusion mode. Hence, it is natural that both kinds of relaxation, two-site and diffusive migration processes, appear in the QENS of the present system. These results also suggest that the two modes are interconnected with each other due to the common elementary jump process between the Tet and adjacent Oct sites. The activation of the effective jump between adjacent Oct sites ($\rho \rightarrow 1$) due to the growing thermal fluctuation with increasing T causes the increase of l in the diffusion mode. This may be evidenced by the closeness of the activation energies of the two modes. This interconnection between the two modes becomes easier to occur with increasing the concentration of H^- at the Oct sites, which leads to the anomalous x' dependence of the diffusion coefficient in $LaH_{x'}$.

Here, we point out that these interconnected dynamics are compatible with a so-called caterpillar model [38] or a concerted migration model [39]. The caterpillar model was originally proposed by Yokota in 1966 [38] to explain the small Haven ratio in fast ion conductors, which describes the deviation from the Einstein relation between mobility and a diffusion constant of a mobile ion. This model allows mobile ions to jump into even an occupied site, which results in introduction of cooperative jumps of several ions [38]. Subsequently, He *et al.* showed that such a concerted migration
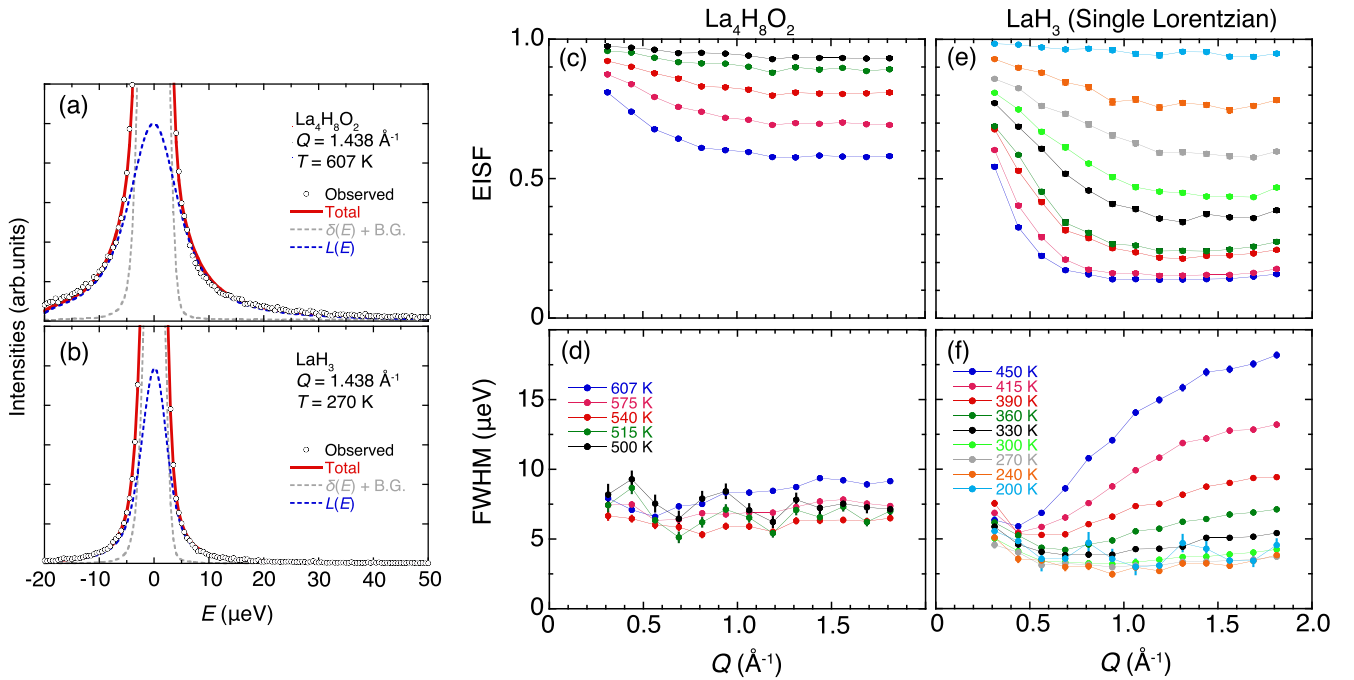
FIG. 4. (a), (b) Typical fitting results of the $S(Q, E)$ spectra for (a) $La_4H_8O_2$ at 607 K and (b) $LaH_{3-\delta}$ at 270 K. A fitting function is composed of the elastic term $\delta(E)$, the single Lorentzian $L(Q, E)$, and the constant background, all of which are convoluted with the resolution function. (c)–(f) Q dependence of EISF [(c), (e)] and FWHM [(d), (f)] for $La_4H_8O_2$ and $LaH_{3-\delta}$, respectively, which are obtained by the fitting to the single Lorenzian. Error bars are estimated from the standard deviations in fitting.

of multiple ions has a lower energy barrier than the original energy barrier determined by the crystal framework, as a result of ion-ion interaction [39]. Although the importance of the cooperative migrations of multiple ions has widely been discussed for a long time in theoretical studies and macroscopic conductivity measurements [40,41], a microscopic experimental evidence for the cooperative migrations is limited. This is partly because the incoherent QENS does not contain direct information about the cooperative migrations.

He *et al.* have also shown in their concerted migration model that there needs to be energetically inequivalent sites for mobile ions with occupancy at a higher energy site [39]. The higher energy site should have locally low barriers and spatially flat energy landscapes, which results in activating the concerted migration of mobile ions with a reduced migration energy barrier [39]. Our Rietveld refinement of the neutron diffraction data for LaD_3 reveals that the isotropic atomic displacement parameter of D at the Oct site is quite large (SM Sec. A [22]). This is consistent with the very shallow potential barrier from the Oct site and the spatially flat energy landscapes. In the case of LaH_3, the isotropic atomic displacement parameter of H at the Oct site would be even larger due to its smaller mass. Also taking into account that the key factor in the high mobility of H^- in $La_4H_yO_{(12-y)/2}$ is a concentration of H^- as stated above, we suggest that the H^- dynamics in LaH_3 are governed by the concerted migration. In candidate materials for a fast ionic conduction governed by the concerted migration mechanism, similar dynamics with simultaneous two-site and diffusive migration processes might be observed by QENS measurements with a suitable timescale.

D. QENS results and H^- dynamics in $La_4H_yO_{(12-y)/2}$ ($y \neq 12$)

Let us move on to the QENS results and the H^- dynamics in $La_4H_yO_{(12-y)/2}$ ($y \neq 12$). In contrast to $LaH_{3-\delta}$, the spectra of $La_4H_8O_2$ even at the highest temperature (607 K) could not be reproduced by the fitting function (1) with reasonable parameters. Therefore, we analyzed the QENS data using a single Lorentzian as a fitting function. Although the spectra are well described by the fitting function with the single Lorentzian as shown in Fig. 4(a), there are some strange features in the parameters obtained: (i) The FWHMs are almost independent of T (and Q) [Fig. 4(d)]. (ii) Although the Q dependence of the FWHM suggests that there is a localized H^- dynamics in $La_4H_8O_2$, the EISF [which is defined as $A_0/(A_0 + A_1)$ in this case, Fig. 4(c)] could not be reproduced by any models that we tried. With forcible fittings, these models provide large distance parameters (>20 Å) despite a localized dynamics.

It is worth mentioning here that the spectra of $LaH_{3-\delta}$ below 270 K are not reproduced by the fitting function with two Lorentzians and that the parameters obtained by the fitting to the single Lorentzian resemble those of $La_4H_8O_2$ [see Figs. 4(e) and 4(f)]. Moreover, when we perform the single Lorentzian fitting to the data of $LaH_{3-\delta}$ above 300 K, the strange feature (i) disappears at the boundary $T \sim 300$ K where the fitting function with two components comes to work. These results indicate that because the FWHM of the L_1 mode starts to enter the resolution limit below 270 K and the intensity of the L_2 mode decreases with decreasing T, the observed QENS spectra are hard to distinguish between the two components. The situation in $La_4H_8O_2$ may be similar to that in $LaH_{3-\delta}$ below 300 K and, therefore, the H^- migrations

would also be similar in $La_4H_yO_{(12-y)/2}$ ($y \neq 12$). As shown in SM Sec. B [22], the results of the mode distribution analysis (MDA), which is a model-free analysis, also confirm the above conjecture.

Even though the H^- dynamics are similar in both $LaH_{3-\delta}$ and $La_4H_8O_2$, there is a large difference in the temperatures that H^- starts to migrate: $T \sim 175$ K in $LaH_{3-\delta}$ and $T \sim 500$ K in $La_4H_8O_2$. This result might be due to the existence of O^{2-} ions as well as the vacant Oct sites. Indeed, the previous MD calculations showed that H^- ions in the vicinity of O^{2-} ions hardly migrate [5,42]. As mentioned in Sec. III C, the incoherent QENS technique does not tell whether these dynamics originate from the concerted migration or individual jumps of H^-. Therefore, the migration mechanism possibly differs between $LaH_{3-\delta}$ and $La_4H_8O_2$, although the QENS results suggest that the H^- dynamics are similar in both $LaH_{3-\delta}$ and $La_4H_8O_2$.

We add that the recent detailed MD simulation for $La_4H_yO_{(12-y)/2}$ ($y \neq 12$) suggests that the H^- diffusion mechanism in $La_4H_yO_{(12-y)/2}$ ($y \neq 12$) considerably differs from that in $LaH_{3-\delta}$ [42]. Our QENS data could not determine such a difference, so further QENS measurements with a slower timescale are highly desirable.

IV. SUMMARY AND CONCLUSION

Our QENS measurements and MD simulations directly determine the two kinds of H^- dynamics in $LaH_{3-\delta}$; the long-range diffusion and the localized jump between the Tet and Oct sites. The MDA results combined with the single Lorentzian fitting results of $La_4H_8O_2$ at 607 K suggest that the H^- dynamics in $La_4H_yO_{(12-y)/2}$ ($y \neq 12$) is similar to that in $LaH_{3-\delta}$. Although our results do not provide direct evidences of the concerted migration mechanism, the following points seem to agree with this mechanism: (i) the key factor in the high mobility of H^- in $La_4H_yO_{(12-y)/2}$ ($y \neq 12$) is a concentration of H^-, (ii) the common elementary jump process of the two modes is the jump between the Tet and adjacent Oct sites, and (iii) the Oct site has the spatially flat energy landscapes. This article provides the detailed microscopic picture of H^- dynamics in $La_4H_yO_{(12-y)/2}$, which results in the anomalous diffusion with high conductivity.

[1] Y. Fukai, *The Metal-Hydrogen System*, Springer Series in Materials Science (GmbH, Springer-Verlag, Berlin,1993).

[2] G. Majer, W. Renz, and R. G. Barnes, J. Phys.: Condens. Matter **6**, 2935 (1994).

[3] U. Stuhr, D. Steinbinder, H. Wipf, and B. Frick, Europhys. Lett. **20**, 117 (1992).

[4] G. Majer, U. Kaess, and R. G. Barnes, Phys. Rev. Lett. **83**, 340 (1999).

[5] K. Fukui, S. Iimura, T. Tada, S. Fujitsu, M. Sasase, H. Tamatsukuri, T. Honda, K. Ikeda, T. Otomo, and H. Hosono, Nat. Commun. **10**, 2578 (2019).

[6] K. Fukui, S. Iimura, A. Iskandarov, T. Tada, and H. Hosono, J. Am. Chem. Soc. **144**, 1523 (2022).

[7] C. Bridges, F. Fernandez-Alonso, J. Goff, and M. Rosseinsky, Adv. Mater. **18**, 3304 (2006).

[8] M. C. Verbraeken, C. Cheung, E. Suard, and J. T. S. Irvine, Nat. Mater. **14**, 95 (2015).

[9] G. Kobayashi, Y. Hinuma, S. Matsuoka, A. Watanabe, M. Iqbal, M. Hirayama, M. Yonemura, T. Kamiyama, I. Tanaka, and R. Kanno, Science **351**, 1314 (2016).

[10] Ø. S. Fjellvåg, J. Armstrong, P. Vajeeston, and A. O. Sjåstad, J. Phys. Chem. Lett. **9**, 353 (2018).

[11] C. Eklöf-Österberg, R. Nedumkandathil, U. Häussermann, A. Jaworski, A. J. Pell, M. Tyagi, N. H. Jalarvo, B. Frick, A. Faraone, and M. Karlsson, J. Phys. Chem. C **123**, 2019 (2019).

[12] F. Takeiri, A. Watanabe, A. Kuwabara, H. Nawaz, N. I. P. Ayu, M. Yonemura, R. Kanno, and G. Kobayashi, Inorg. Chem. **58**, 4431 (2019).

[13] H. Ubukata, T. Broux, F. Takeiri, K. Shitara, H. Yamashita, A. Kuwabara, G. Kobayashi, and H. Kageyama, Chem. Mater. **31**, 7360 (2019).

[14] H. Ubukata, F. Takeiri, K. Shitara, C. Tassel, T. Saito, T. Kamiyama, T. Broux, A. Kuwabara, G. Kobayashi, and H. Kageyama, Sci. Adv. **7**, eabf7883 (2021).

[15] M. Bee, *Quasielastic Neutron Scattering* (Hilger, Bristol, 1988).

[16] R. Hempelmann, *Quasielastic Neutron Scattering and Solid State Diffusion* (Clarendon, Oxford, 2000).

[17] K. Shibata, N. Takahashi, Y. Kawakita, M. Matsuura, T. Yamada, T. Tominaga, W. Kambara, M. Kobayashi, Y. Inamura, T. Nakatani, K. Nakajima, and M. Arai, JPS Conf. Proc. **8**, 036022 (2015).

[18] K. Nakajima, S. Ohira-Kawamura, T. Kikuchi, M. Nakamura, R. Kajimoto, Y. Inamura, N. Takahashi, K. Aizawa, K. Suzuya, K. Shibata, T. Nakatani, K. Soyama, R. Maruyama, H. Tanaka, W. Kambara, T. Iwahashi, Y. Itoh, T. Osakabe, S. Wakimoto, K. Kakurai, F. Maekawa, M. Harada, K. Oikawa, R. E. Lechner, F. Mezei, and M. Arai, J. Phys. Soc. Jpn. **80**, SB028 (2011).

[19] Y. Inamura, T. Nakatani, J. Suzuki, and T. Otomo, J. Phys. Soc. Jpn **82**, SA031 (2013).

[20] R. T. Azuah, L. R. Kneller, Y. Qiu, P. L. W. Tregenna-Piggott, C. M. Brown, J. R. D. Copley, and R. M. Dimeo, J. Res. Natl. Inst. Stand. Technol. **114**, 341 (2009).

[21] J. Rodriguez-Carvajal, Phys. B: Condens. Matter **192**, 55 (1993).

[22] See Supplemental Material at http://link.aps.org/supplemental/10.1103/PhysRevB.107.184114 for the crystal structure analysis of LaH_3 and its temperature dependence; the results of mode distribution analyses; fitting results for $LaH_{3-\delta}$ in other models; the characteristic temperature at which H^- ions start to migrate in $LaH_{3-\delta}$; DFT-based neural network potential for $LaH_{3-\delta}$; mean square displacements in LaH_3 and $LaH_{3-\delta}$ calculated with NNP-MD simulation; results of the potential barrier calculation by the climbing image nudged elastic band method (CI-NEB); QENS results of $La_4H_6O_3$ and $La_4H_4O_4$; and the results of AMATERAS. The Supplemental Material also includes Refs. [43–48].

[23] K. Momma and F. Izumi, J. Appl. Crystallogr. **44**, 1272 (2011).

[24] W. L. Korst and J. C. Warf, Inorg. Chem. **5**, 1719 (1966).

[25] H. Mizoguchi, M. Okunaka, M. Kitano, S. Matsuishi, T. Yokoyama, and H. Hosono, Inorg. Chem. **55**, 8833 (2016).

[26] C. T. Chudley and R. J. Elliott, Proc. Phys. Soc. **77**, 353 (1961).

[27] C. Elsässer, K. M. Ho, C. T. Chan, and M. Fähnle, J. Phys.: Condens. Matter **4**, 5207 (1992).

[28] Y. Li and G. Wahnström, Phys. Rev. B **46**, 14528 (1992).

[29] H. Kimizuka, S. Ogata, and M. Shiga, Phys. Rev. B **97**, 014102 (2018).

[30] H. Kimizuka, S. Ogata, and M. Shiga, Phys. Rev. B **100**, 024104 (2019).

[31] P. Hagenmuller, J. M. Reau, C. Lucat, S. Matar, and G. Villeneuve, Solid State Ionics **3-4**, 341 (1981).

[32] S. I. Campbell, M. Kemali, D. K. Ross, D. J. Bull, J. F. Fernandez, and M. R. Johnson, J. Alloys Compd. **293-295**, 351 (1999).

[33] A. V. Skripov, M. Pionke, O. Randl, and R. Hempelmann, J. Phys.: Condens. Matter **11**, 1489 (1999).

[34] A. V. Skripov, T. J. Udovic, and J. J. Rush, Phys. Rev. B **76**, 104305 (2007).

[35] J. Behler and M. Parrinello, Phys. Rev. Lett. **98**, 146401 (2007).

[36] A. Singraber, J. Behler, and C. Dellago, J. Chem. Theory Comput. **15**, 1827 (2019).

[37] G. Henkelman, B. P. Uberuaga, and H. Jónsson, J. Chem. Phys. **113**, 9901 (2000).

[38] I. Yokota, J. Phys. Soc. Jpn. **21**, 420 (1966).

[39] X. He, Y. Zhu, and Y. Mo, Nat. Commun. **8**, 15893 (2017).

[40] C. E. Mohn, N. L. Allan, C. L. Freeman, P. Ravindran, and S. Stølen, Phys. Chem. Chem. Phys. **6**, 3052 (2004).

[41] E. Kendrick, J. Kendrick, K. S. Knight, M. S. Islam, and P. R. Slater, Nat. Mater. **6**, 871 (2007).

[42] A. Iskandarov, T. Tada, S. Iimura, and H. Hosono, Acta Mater. **230**, 117825 (2022).

[43] T. Kikuchi, K. Nakajima, S. Ohira-Kawamura, Y. Inamura, O. Yamamuro, M. Kofu, Y. Kawakita, K. Suzuya, M. Nakamura, and M. Arai, Phys. Rev. E **87**, 062314 (2013).

[44] Y. Kawakita, T. Kikuchi, S. Tahara, M. Nakamura, Y. Inamura, K. Maruyama, Y. Yamauchi, S. Ohira-Kawamura, and K. Nakajima, JPS Conf. Proc. **33**, 011071 (2021).

[45] G. Kresse and J. Furthmüller, Phys. Rev. B **54**, 11169 (1996).

[46] G. Kresse and J. Furthmüller, Comput. Mater. Sci. **6**, 15 (1996).

[47] P. E. Blöchl, Phys. Rev. B **50**, 17953 (1994).

[48] J. P. Perdew, K. Burke, and M. Ernzerhof, Phys. Rev. Lett. **77**, 3865 (1996).